Aerothermoelasticity: Its Impact on Stability and Control of Winged Aerospace Vehicles

JOHN H. WYKES* AND ROBERT E. LAWRENCE†
North American Aviation, Inc., Los Angeles, Calif.

Many aerospace vehicles of current interest have low load factor-low mass fraction structure that induces aerothermoelastic problems of broad impact on vehicle design and must, therefore, be assessed early in the design cycle. Attention in this study has been directed to aerothermoelastic effects associated with the longitudinal stability and control of a possible supersonic transport canard-delta configuration. Flexible-to-rigid-ratio data obtained from modal techniques are presented for most major aerodynamic parameters at two loading conditions. Distribution of mass is shown to be the major source of significant differences obtained. A direct influence coefficient approach provided additional insight into component mass and aerodynamic influences. Particular attention is drawn to the large impact of pitch inertia loadings on effective static stability and the resultant effects on the vehicle short-period dynamics. A wide range of design compromises is shown to be available to the designer through positive use of the flexible vehicle's mass and aerodynamic characteristics. It is concluded that most efficient use of weight in vehicle design will only be achieved through coordinated and detailed examination of the aerothermoelastic problem areas early in the design cycle. Additional research and development effort to this end is recommended.

Nomenclature‡

S_w	= wing area
$\bar{c}_w$	= wing mean aerodynamic chord
$l_c/\bar{c}_w$, $x_w/\bar{c}_w$, $x_e/\bar{c}_w$	= nondimensional moment arms of canard, wing, and elevon loads, respectively
m	= vehicle mass, W/g
I_y	= pitch inertia
g	= acceleration of gravity
V_0	= velocity
q_0	= dynamic pressure
q_{0D}	= divergence dynamic pressure
α	= angle of attack of reference plane
$\dot{\alpha}$	= rate of change of angle of attack
α_w	= angle of attack of the wing
α_c	= canard angle of attack
γ	= incremental change in canard angle of attack due to fuselage bending
$d\gamma/dL_c$, $d\gamma/dn$	= fuselage bending due to canard load and load factor, respectively
Θ, θ	= Euler pitch angle
q	= pitch rate, $d\theta/dt$
$\ddot{\theta}$	= pitch acceleration, $d\theta^2/dt^2$, $\dot{q}$
δ_c	= canard deflection
δ_e	= elevon deflection
η_i	= generalized coordinate, structural mode i
$\dot{\eta}_i$	= velocity of generalized coordinate, structural mode i
$\ddot{\eta}_i$	= acceleration of generalized coordinate, structural mode i
g_s	= structural damping coefficient
ω_i	= natural frequency, structural mode i
M_i	= generalized mass, structural mode i
ω_{n_0}	= undamped natural frequency
ζ	= damping ratio
ω_n	= natural frequency
C_L	= lift coefficient ($C_L \approx C_N$)
C_N	= normal force coefficient
C_{L_α}	= lift curve slope, $\partial C_L/\partial\alpha$
C_{N_α}	= normal force curve slope, $\partial C_N/\partial\alpha$
$C_{L_{\alpha_c}}$	= canard lift curve slope
$C_{L_{\alpha_w}}$	= wing lift curve slope
$C_{L_{\delta_e}}$	= elevon deflection lift effectiveness
$C_{N_{\delta_e}}$	= elevon deflection normal force effectiveness
$C_{N_{\delta_c}}$	= canard deflection normal force effectiveness
$C_{N_{(\alpha=0)}}$	= normal force coefficient at $\alpha = 0$
C_{N_q}	= normal force due to pitching, $\partial C_N/[\partial(q\bar{c}_w/2V_0)]$
$C_{NI_{\alpha_c}}$	= canard interference normal force curve slope (acts on wing)
$C_{NI_{\delta_c}}$	= canard deflection interference normal force effectiveness
$C_{N_{\ddot{\theta}}}$	= normal force coefficient due to pitching acceleration, $\partial C_N/\partial\ddot{\theta}$
$C_{N_{\eta_i}}$	= normal force due to ith mode deflection
C_m	= pitching moment coefficient
C_{m_α}	= pitching moment curve slope, $\partial C_m/\partial\alpha$
$C_{m_{\alpha_c}}$	= pitching moment due to canard angle of attack
$C_{m_{\delta_e}}$	= elevon deflection pitching moment effectiveness
$C_{m_{\delta_c}}$	= canard deflection pitching moment effectiveness
$C_{m_{(\alpha=0)}}$	= pitching moment coefficient at $\alpha = 0$
C_{m_q}	= pitching moment due to pitching, $\partial C_m/[\partial(q\bar{c}_w/2V_0)]$
$C_{mI_{\alpha_c}}$	= canard interference pitching moment curve slope
$C_{mI_{\delta_c}}$	= canard deflection interference pitching moment effectiveness
$C_{m_{\ddot{\theta}}}$	= pitching moment coefficient due to pitching acceleration, $\partial C_m/\partial\ddot{\theta}$
$C_{m_{\eta_i}}$	= pitching moment coefficient to ith mode deflection
$(\partial C_m/\partial C_L)_{\text{eff}}$	= effective static stability
C_{η_i}	= generalized force coefficient in ith mode
$C_{\eta_{i_\alpha}}$	= generalized normal force coefficient in the ith mode due to angle of attack, $\partial C_{\eta_i}/\partial\alpha$
$C_{\eta_i\eta_j}$	= generalized force coefficient in the ith mode due to jth mode deflection, $\partial C_{\eta_i}/\partial C_{\eta_j}$
$[\ ]_F$	= flexible state of bracketed item
$[\ ]_R$	= rigid state of bracketed item

Presented as Preprint 64-489 at the 1st AIAA Annual Meeting, Washington, D. C., June 29–July 2, 1964; revision received January 4, 1965.

* Senior Technical Specialist, Project Dynamics, Structures Technology, Engineering. Associate Fellow Member AIAA.

† Senior Technical Specialist, Aerodynamics, Flight Technology, Engineering.

‡ Standard stability and body axes systems are used. To avoid confusion, it should be noted that the stability axes C_L and the body axes C_N are positive in the up direction, whereas the body axes generalized coordinate η_i and the coefficients $C_{\eta_{i\alpha}}$, C_{η_i}, and $C_{\eta_i\eta_j}$ are positive in the down direction.

Introduction

DURING the preliminary design cycle of a new aerospace vehicle, it is important to provide proper emphasis to all first-order factors affecting the vehicle's ultimate flight performance. In recent years, a number of vehicles have had aerothermoelastic characteristics become one of these first-order factors. Partly responsible for this situation has been the demand for high-speed performance at flight conditions producing high heat input to the vehicle structure. These mission requirements result in structural design features such as thin lifting surfaces and high fineness ratio fuselages having high flexibility. Also affecting the flexibility of many designs of interest are a low load factor requirement and a low mass fraction structure ($W_{\text{struct}}/W_{T.O.\text{gross}}$) resulting from the use of high design stresses. Although any one vehicle may not combine all of these flexibility-producing factors, a sufficient number may be present to be of concern. Two types of vehicles of current interest which combine a significant number of these flexibility factors are the supersonic transport and the space transport. For such designs, it is no longer sufficient to provide structure at the preliminary design level to meet strength requirements only; sufficient structural material must also be provided to meet stiffness requirements for assuring satisfactory structural dynamics (flutter, landing loads, etc.) and stability and control characteristics.[1] It is not difficult to see, then, that a first-order weight accounting with its attendant impact on speed and range performance must include aerothermoelastic considerations. As already intimated, aerothermoelasticity makes itself felt in the two major design areas of structural dynamics and stability and control. It is the primary intent of this paper to emphasize the potential effects of aerothermoelasticity on vehicle stability and control. All vehicles, be they canard-delta, simple delta, or a tail-aft configuration, will experience these effects; however, the results of a study of the typical canard-delta configuration of Fig. 1 are discussed herein as a specific illustrative example. Only the longitudinal design area is covered; the techniques developed, though, are also applicable to the lateral-directional design area. The detailed objectives of this study were threefold: 1) to provide the aerodynamic and structural configuration designer with techniques that would permit visual insight into the impact of the aerothermoelastic effects on various vehicle components and complete vehicle aerodynamic characteristics, 2) to provide a relatively simple technique for including all major inertial and aerodynamic effects on the flexible vehicle for the purpose of checking flying qualities and control system design, and 3) to probe and assess potentially important aerothermoelastic problem areas.

In obtaining these objectives, two analysis techniques were developed: a modal technique and a direct influence coefficient technique. Both of these approaches to defining the aerothermoelastic characteristics of the vehicle provided unique insight that aided in obtaining design objectives.

Analysis Techniques

To provide a meaningful background against which aerothermoelastic design problems may be discussed, a short review is given here of the two types of analysis techniques used; that is, the modal technique and the direct influence coefficient technique. These two methods have common elements that should be emphasized. The structural description of the vehicle is defined by a set of influence coefficients. These influence coefficients are used together with the vehicle's mass characteristics in a free vibration analysis to obtain the normal modes that are the basis of the modal technique. The direct influence coefficient technique derives its name from the fact that the influence coefficients enter the aerothermoelastic analysis without this intermediate processing. Both of these approaches utilize the same rigid vehicle load distributions and the same techniques to describe the quasi-steady aerodynamic loads developed by the deformed structure.

Modal Technique

The structural deflections arising in this technique are described through the superposition of the normal modes of free vibration of the vehicle; in theory an infinite number are required, but in practice a reasonable number will suffice. For the vehicle of this study, four symmetric modes appeared to give good accuracy when matched against static structural deformations obtained using structural influence coefficients. Other vehicles would need to be checked in this manner to ascertain the correct number of free vibration modes to meet their individual accuracy needs.

The use of the modal approach in aeroelastic problems is not new; it has received wide acceptance in flutter analyses.[2,3] Its use has been much less extensive in connection with stability and control types of analyses. It will be shown, however, that the modal approach has much to recommend it for analyses of the aerothermoelastic effects on stability and control of very flexible air vehicles such as the one studied. The major advantages may be summed up by saying that the approach provides a concise, economical framework for including all important inertial and aerodynamic loadings. In addition, the form of the aerodynamic data may be cast in such a manner as to provide perspective to pertinent current design problem areas.

In the modal context, the longitudinal-symmetric equations of motion suitable for a dynamic stability and control problem analysis appear in a general form as follows (a body axes system is used):

Rigid body plunge mode

$$\dot{\alpha} = +q + (g/V_0)\cos\Theta - (q_0 S_w/mV_0)[C_{N_{\text{rigid}}} + \Delta C_{N_{\text{flexible}}}]$$

Rigid body pitch mode

$$\dot{q} = (q_0 S_w \bar{c}_w/I_y)[C_{m_{\text{rigid}}} + \Delta C_{m_{\text{flexible}}}]$$

Structural symmetric modes

$$\ddot{\eta}_i = -g_s\omega_i\dot{\eta}_i - \omega_i^2\eta_i + (q_0 S_w/M_i)[(C_{\eta_i})_{\text{rigid}} + (\Delta C_{\eta_i})_{\text{flexible}}]$$

As shown, the rigid aerodynamic components appear as separate contributions. Let us expand the aerodynamic part of these equations but restrict ourselves, for simplicity of explanation, to the consideration of only two airplane components: 1) the wing-body and 2) the canard. In addition, assume (again, for simplicity) that the rigid body motion and the structural motion will be slow enough that structural acceleration ($\ddot{\eta}_i$) and structural velocity ($\dot{\eta}_i$) will be negligibly small:

$$[C_{N_{\text{rigid}}} + \Delta C_{N_{\text{flexible}}}] = \underbrace{(C_{N_\alpha})_{\text{wing-body}}\,\alpha + (C_{N_{\alpha_c}})_{\text{canard}}\alpha_c}_{\text{rigid aero}} + \underbrace{C_{N_{\eta_1}}\eta_i + C_{N_{\eta_2}}\eta_2 + C_{N_{\eta_3}}\eta_3 + C_{N_{\eta_4}}\eta_4}_{\text{flexible correction}}$$

$$[C_{m_{\text{rigid}}} + \Delta C_{m_{\text{flexible}}}] = \underbrace{(C_{m_\alpha})_{\text{wing-body}}\alpha + (C_{m_{\alpha_c}})_{\text{canard}}\alpha_c}_{\text{rigid aero}} + \underbrace{C_{m_{\eta_1}}\eta_i + C_{m_{\eta_2}}\eta_2 + C_{m_{\eta_3}}\eta_3 + C_{m_{\eta_4}}\eta_4}_{\text{flexible correction}}$$

$$[(C_{\eta_i})_{\text{rigid}} + (\Delta C_{\eta_i})_{\text{flexible}}] = \underbrace{(C_{\eta i_\alpha})_{\text{wing-body}}\alpha + (C_{\eta i_{\alpha_c}})_{\text{canard}}\alpha_c}_{\text{rigid aero}} + \underbrace{C_{\eta i_{\eta_1}}\eta_1 + C_{\eta i_{\eta_2}}\eta_2 + C_{\eta i_{\eta_3}}\eta_3 + C_{\eta i_{\eta_4}}\eta_4}_{\text{flexible correction}}$$

As is seen from the form of these data, the flexibility corrections are lumped, and individual component flexibility corrections are not readily broken out and associated with the appropriate rigid load. For most stability and control problem descriptions where solutions to the equations are the primary goals, this concise formulation is highly desirable. However, from the point of view of the aerodynamic and structural designer who wishes to identify component contributions in order to make intelligent design decisions, this concise form is a hindrance. To provide the desired important design visibility, the aerodynamic data were linearized, and flexible-to-rigid-ratio aerodynamic corrections were generated using modal data. These ratios themselves provided important design information, but they also were most useful in providing a pictorial comparison of vehicle component and complete vehicle flexible and rigid aerodynamic characteristics, as will be demonstrated.

In order to form the desired flexible-to-rigid ratios for correcting the rigid data, the individual aerodynamic components must be broken out. With the assumption of linearity of the rigid aerodynamic data and its companion property of allowing superposition of component answers to form the total, this can be done as described below.

The modal equations for the symmetric modes associated with the longitudinal equations of motion take the displayed form under the assumption of quasi-steady conditions:

$$\eta_i = (q_0 S_w/\omega_i^2 M_i)[\underbrace{(C_{\eta_{i_\alpha}})_{\text{wing-body}}\,\alpha + (C_{\eta_{i_{\alpha_c}}})_{\text{canard}}\,\alpha_c}_{\text{rigid aero}} + \underbrace{C_{\eta_{i\eta_1}}\eta_1 + C_{\eta_{i\eta_2}}\eta_2 + C_{\eta_{i\eta_3}}\eta_3 + C_{\eta_{i\eta_4}}\eta_4}_{\text{flexible correction}}]$$

If all but one of the rigid aero inputs to the modal equations were removed, one would obtain the modal response in all four modes for that particular loading. These modal responses, in turn, can be used to determine the amount of the flexibility input caused by that component in the force and moment equations. Consider the wing-body component of normal force due to angle of attack in mode 1 as an example of the simultaneous equation format:

$$[C_{\eta_{1\eta_1}} - (\omega_i^2 M_i/q_0 S_w)]\eta_i + C_{\eta_{1\eta_2}}\eta_2 + C_{\eta_{1\eta_3}}\eta_3 + C_{\eta_{1\eta_4}}\eta_4 = -(C_{\eta_{1_\alpha}})_{\text{wing-body}}\,\alpha$$

It will be noted that the left side of a set of simultaneous modal equations set up as in the foregoing example remains unchanged for a given Mach number-altitude condition and a given structural definition. The $C_{\eta_{i\eta_j}}$ terms are coupling terms among the modes and are independent of the rigid aerodynamic loadings. The right sides of the equations represent the particular rigid aero loading for which the flexible-to-rigid ratio is sought.

Solving this set of simultaneous equations, η_1 through η_4 are obtained due to the inputs $(C_{\eta_{1_\alpha}})_{\text{wing-body}}\alpha$ through $(C_{\eta_{4_\alpha}})_{\text{wing-body}}\,\alpha$ which are associated with the rigid airload $(C_{N_\alpha})_{\text{wing-body}}\,\alpha$. The flexible vehicle airload and moment are now obtained using these responses:

$$C_{N_{\text{flexible}}} = C_{N_{\text{rigid}}} + C_{N_{\eta_1}}\eta_1 + C_{N_{\eta_2}}\eta_2 + C_{N_{\eta_3}}\eta_3 + C_{N_{\eta_4}}\eta_4$$

$$C_{m_{\text{flexible}}} = C_{m_{\text{rigid}}} + C_{m_{\eta_1}}\eta_1 + C_{m_{\eta_2}}\eta_2 + C_{m_{\eta_3}}\eta_3 + C_{m_{\eta_4}}\eta_4$$

It is easy now to form a flexible-to-rigid ratio for these wing-body force and moment components:

$$\frac{[C_{N_\alpha}]_{\text{flexible}}}{[C_{N_\alpha}]_{\text{rigid}}} = \frac{C_{N_{\text{flexible}}}}{C_{N_{\text{rigid}}}} = 1 + \frac{C_{N_{\eta_1}}\eta_1 + C_{N_{\eta_2}}\eta_2 + C_{N_{\eta_3}}\eta_3 + C_{N_{\eta_4}}\eta_4}{C_{N_{\text{rigid}}}}$$

$$\frac{[C_{m_\alpha}]_{\text{flexible}}}{[C_{m_\alpha}]_{\text{rigid}}} = \frac{C_{m_{\text{flexible}}}}{C_{m_{\text{rigid}}}} = 1 + \frac{C_{m_{\eta_1}}\eta_1 + C_{m_{\eta_2}}\eta_2 + C_{m_{\eta_3}}\eta_3 + C_{m_{\eta_4}}\eta_4}{C_{m_{\text{rigid}}}}$$

Attention is again directed to the very important fact that, since normal modes (both rigid body and structural) are used, the structural responses (η_i's) obtained in the manner just described reflect loading of the *free structure* under the *aerodynamic load* being considered and the *corresponding inertia load* resulting from application of this aerodynamic load to the unrestrained vehicle.

Direct Influence Coefficient Technique

In the direct influence coefficient technique, the vehicle can be conveniently separated into components such as wing, fuselage, and canard. The influence of aerothermoelasticity on an individual component is determined for each of its various loadings. The complete flexible vehicle is then described as a summation of inputs of the components. The principal advantage of the direct influence coefficient over the modal approach is the inherent capability for permitting separation of inertial loading effects from aerodynamic loading effects.

Structural description of a lifting surface is provided by flexibility (deflection) influence coefficients. Temperature effects are included in the influence coefficients, and several sets may be required for a complete description when severe aerodynamic heating is present.

The individual lifting surface aerodynamic characteristics are studied by a technique that is fundamentally a conventional assumed mode static aeroelastic analysis. Extensive treatment of this procedure in the literature precludes the need for detailed description.[3,4] The present discussion will accordingly be restricted to consideration of particular assumptions and variations pertinent only to this subject analysis. The incremental aerodynamic loadings associated with the assumed modes may be derived from any convenient theoretical or experimental source. For low-aspect-ratio components, a lifting surface theory, such as Falkner (subsonic) or Etkin/Evvard (supersonic), is appropriate.[5,6] Solution is accomplished by an iteration process employing a forced convergence. Accuracy of convergence is assured by checks of each individual load as well as total load and total moments. The influence of flexibility is described in terms of flexible-to-rigid ratios or flexible increments of the rigid parameter.

Procedures for combining the component data to describe the complete flexible vehicle are well known and will not be detailed here. One exception may be found in the treatment of inertia effects. As will be discussed later, significant variations have been noted in the aeroelastic parameters resulting from inertia loadings, and it can be shown that these variations are dependent only on distribution and not magnitude. To facilitate studies of mass distribution phenomena

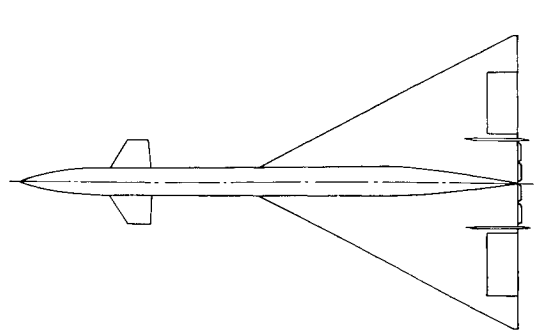

Fig. 1 A possible canard-delta supersonic transport configuration.

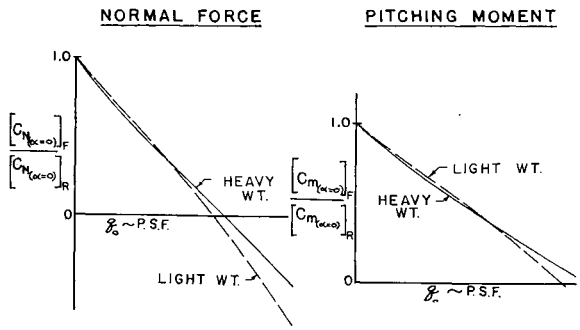

Fig. 2 Wing-body component, flexible-to-rigid ratios for zero angle-of-attack characteristics vs dynamic pressure at a high subsonic Mach number.

and aid in rapid evaluation of any particular weight condition, the total mass of the vehicle was subdivided into elements. Two classes of mass elements were considered: 1) fixed weight, such as structure, engines, etc.; and 2) variable weight, such as fuel or other payload. The number of elements normally depend on the physical constraints of the vehicle and the degree of versatility desired in the study. Aeroelastic parameters generated for the various mass elements could be combined to describe the net effect for any desired gross weight and/or weight distribution conditions. Within this framework, procedures were developed to define the following in addition to any prespecified weight condition:

maximum forward center of gravity, maximum aft center of gravity } specified gross weight

maximum static margin, minimum static margin } specified gross weight and center of gravity

Aerothermoelastic Effects on Longitudinal Stability and Control Parameters

Application of the preceding modal technique to the canard-delta configuration of Fig. 1 at a high subsonic Mach number produced the flexible-to-rigid data shown in Figs. 2–7. A high subsonic Mach number flight condition was chosen for the study, since most aerothermoelastic effects become critical in this flight regime. Stability and control parameter data for two weight configurations are shown: a heavy-weight (full-fuel) case and a light-weight (no-fuel) case. Before discussing the trend of each individual aerodynamic parameter, a general comment about the interpretation of the free vehicle response under loading is in order. Just as the deflection pattern of a simply supported beam is determined by the net running loads and moments acting, so, too, is the deflection pattern of the free flying air vehicle. In the case of the air vehicle, both inertial and aerodynamic loads contribute to the net running loads and moments. If the mass distributions for the two different weight conditions are identical, the fixed distribution aerodynamic load required for maintaining a balance will be in proportion to the weights and will produce identical running load distributions that are in proportion to the weights. In the context of the technique used to get flexible-to-rigid ratios, a unit load applied on the different weight-free structures induces identical running loads. Viewed as (force) = (mass) × (acceleration), the heavier vehicle would not accelerate as fast as the light vehicle, but the (mass) × (acceleration) magnitude still equals the fixed applied force. Thus it can be said that the differences in the flexible aerodynamic data to be noted for the two different weight conditions are attributable to mass *distribution* and not mass magnitude.

Figure 2 shows the flexibility impact on the normal force and pitching moment characteristics at zero angle of attack. Little effect due to mass distribution was evident, but marked sensitivity with dynamic pressure increase was obtained. It is very difficult to assign a primary reason for the trends noted for these parameters (as can be done for those parameters to follow) because the rigid distributed loading is a complicated pattern. About all that can be said is that the original negative normal force distribution in conjunction with the two levels of mass distribution bent the free vehicle in a manner to induce a positive angle of attack on the wing always. The positive normal force, being aft of the center of gravity, produced a negative pitching moment opposing the original rigid positive moment component.

The flexible-to-rigid curves for the wing-body components of the normal force and pitching moment angle-of-attack derivatives are shown in Fig. 3. Mass distribution is shown to have a highly significant effect on these parameters. In the light-weight condition, increasing dynamic pressure produced a trend toward moderate increases in lift and marked increases in pitching moment; in the heavy-weight condition, trends opposite to those for the light-weight case were obtained. The trends indicated for these two parameters have significant implications for the vehicle's static and dynamic stability, as will be discussed. The following observations help to provide an appreciation for these particular data trends. The net running load on the light-weight flexible configuration produced a deflection pattern that humped in the center when viewed from the side. Since the wing was located aft, a net positive angle of attack resulted which produced the increased normal force with dynamic pressure increase. The canard was located on the negative angle of attack part of the forward fuselage and produced a negative normal force. This force, however, was small as compared to the positive induced wing normal force. It is also pertinent, though, to note that this negative canard normal force was a potent factor in determining the vehicle bending pattern obtained and, as such, was largely responsible for the observed positive normal force increase generated by the wing. The heavy-weight configuration

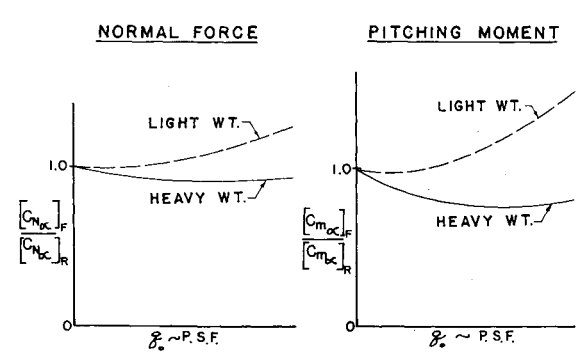

Fig. 3 Wing-body component, angle-of-attack derivative flexible-to-rigid ratios vs dynamic pressure at a high subsonic Mach number.

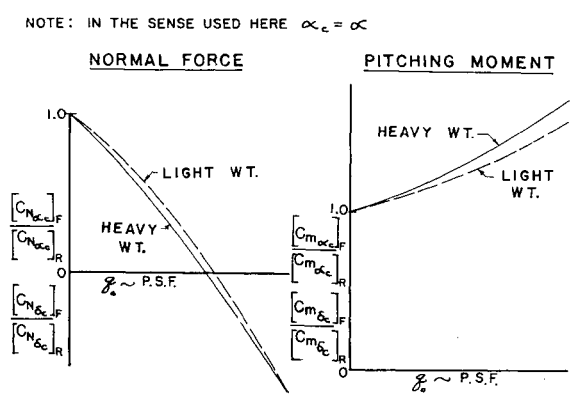

Fig. 4 Canard component, angle-of-attack derivative flexible-to-rigid ratios vs dynamic pressure at a high subsonic Mach number.

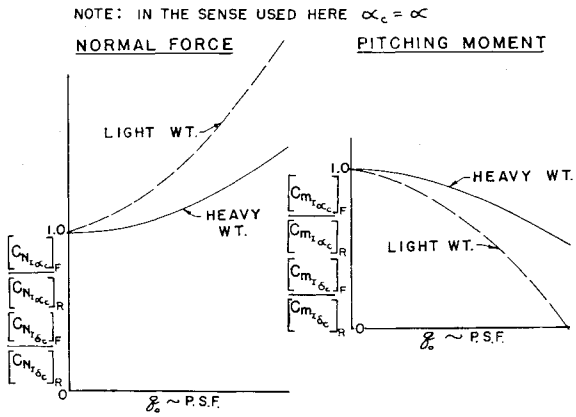

Fig. 5 Canard-wing interference component, angle-of-attack derivative flexible-to-rigid ratios vs dynamic pressure at a high subsonic Mach number.

developed a deflection pattern opposite to that of the light-weight configuration, and therefore reasoning similar to that just reviewed explains the data trends for this configuration.

The influence of flexibility on the rigid canard normal force and pitching moment contributions are presented in Fig. 4. A small mass distribution effect was obtained, together with a marked decrease in normal force and a large increase in pitching moment with increasing dynamic pressure. The explanation for this is that rigid positive canard load induced a running load on the free vehicle which formed a deflection pattern inducing a large negative angle of attack on the wing; it is the resulting large negative normal force and positive pitching moment that are reflected in the data shown.

A positive normal force on a canard located on a vehicle as shown in Fig. 1 induces a negative normal force on the inboard portion of the wing through the canard downwash pattern which, because of center of pressure location ahead of the c.g., produces a negative pitching moment. As Fig. 5 indicates, relatively large effects of flexibility were obtained which modified this interference loading, more so for the light-weight configuration than for the heavy. This interference load distribution was such that the net bending pattern produced a small positive canard load and a large negative wing load aft of the c.g., and both loads developed pitching moment inputs that were positive and thus reduced the original rigid negative moment.

The effect of flexibility on elevon normal force and pitching moment effectiveness was large, as indicated in Fig. 6. The effect of mass distribution on these parameters was small. This latter result may be attributed to the fact that in both weight conditions the mass loads tended to cluster about the c.g. (less so for the light-weight case), and the elevon forces on both configurations loaded up the aft end. The resulting running loads on the free structure did have differences, but

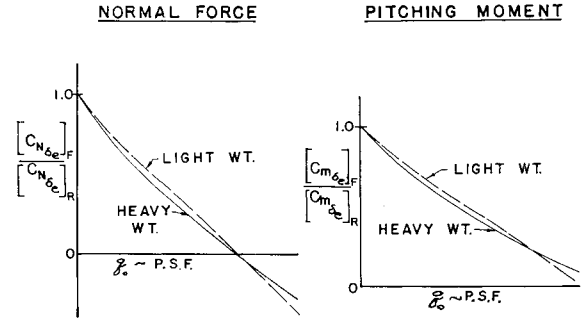

Fig. 6 Elevon component, deflection derivative flexible-to-rigid ratios vs dynamic pressure at a high subsonic Mach number.

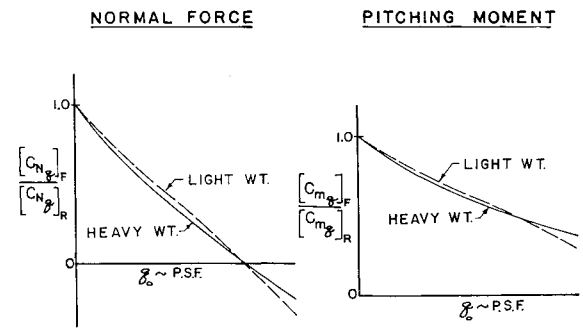

Fig. 7 Wing-body component, pitch rate derivative flexible-to-rigid ratios vs dynamic pressure at a high subsonic Mach number.

only of magnitudes to introduce minor variations in the flexible normal force and pitching moment response.

The flexible-to-rigid ratios for the normal force due to pitching and the pitching moment due to pitching (damping in pitch) are given in Fig. 7. Large changes with increasing dynamic pressure were obtained, whereas only minor changes due to the mass distribution were evident. Note the similarity between these curves and the elevon effectiveness curves in Fig. 6. The source of this similarity is identified when attention is called to the fact that both have highly loaded trailing edges. This rigid load developed for the pitching case takes the shape it does because the local induced angles of attack are proportional to the distance from the center of gravity. The net vehicle loading, then, is similar to that for the elevon case, and the logic used there to explain trends is applicable here.

A word about the treatment of the canard surface flexibility is in order. In this study, the structural frequency magnitudes of the canard were far enough removed from the lower vehicle frequencies so that no large dynamic coupling could be present. The surface flexibility was important, however, and was accounted for by the flexible-to-rigid ratio of Fig. 8. Note that, for the relatively low sweep angle of the quarter chord of the canard surface of Fig. 1, flexibility effects increased the lift curve slope. In all of the previous data where canard inputs were indicated, all of the rigid values could really be interpreted as including this surface flexibility; for instance, $[C_{N_{\alpha_c}}]_{\text{rigid}} = K_c(C_{N_{\alpha_c}})_{\text{rigid}}$. This fact is particularly pertinent when constructing the complete vehicle flexible normal force and pitching moment curves.

Having the vehicle's component flexible-to-rigid ratios, the complete vehicle's flexible characteristics may be presented graphically. As examples of this, the complete vehicle's normal force and pitching moment characteristics as a function of angle of attack were constructed. Figure 9 presents the normal force curve data for the two weight conditions studied at sea level. Looking at the complete vehicle curves, it is noted that flexible heavy-weight configuration has a lower curve slope than does the flexible light-weight configuration. Comparisons of the component contributions to

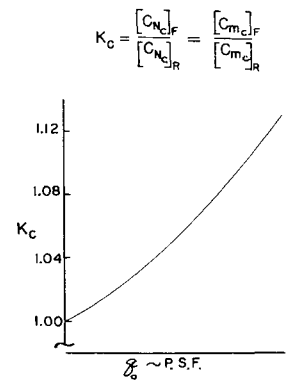

Fig. 8 Canard surface flexible-to-rigid ratio at a high subsonic Mach number.

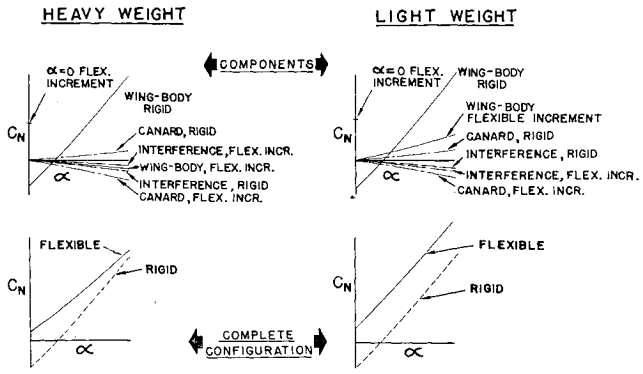

Fig. 9 Normal force vs angle-of-attack buildup, flexible and rigid airplane at a high subsonic Mach number; sea-level flight condition.

the complete vehicle curves identify immediately the cause for the differences noted; it is the previously discussed wing-body contribution of Fig. 3. Figure 10 presents the pitching moment curve data for the components and the complete vehicle. A very marked effect of mass distribution is noted for the complete flexible vehicle; the light-weight configuration indicates static stability nearly comparable to the rigid vehicle, whereas the heavy-weight configuration borders on neutral stability. Again, the component breakdown presented in Fig. 10 identifies the major cause of the differences observed, namely, the wing-body contribution.

Use of the modal technique in describing aerothermoelastic effects on flexible vehicles has been shown to be highly useful. One of the prime advantages has been its ability to include *inertia loadings* automatically through the use of the free vehicle normal modes. In assessing the relative magnitude of inertia to aerodynamic loadings in aerothermoelastic parameters, this automatic feature is a hindrance; the direct influence coefficient method of analyses then has an advantage in this context in that individual loadings (including inertia) must be explicitly added to the equations describing the flexible vehicle response.

The direct influence coefficient techniques were used in this study to demonstrate the importance of various loadings (but emphasizing inertia loadings) on the vehicle speed stability (control surface deflection required to trim at 1.0-g level flight at various Mach numbers), accelerated longitudinal stability (control deflection required vs load factor at a given Mach number-altitude condition), and short-period frequency characteristics. Although there are other parameters entering the analyses of these vehicle characteristics, the attention of this phase of the study was oriented toward identifying the contributions of combined translational acceleration and angle-of-attack aerodynamics, pitch damping, and pitch acceleration inertia loadings to what has been identified as "effective static stability," $(\partial C_m/\partial C_L)_{\text{eff}}$. The aptness of this nomenclature will become more apparent as the discussion continues.

To illustrate how the $(\partial C_m/\partial C_L)_{\text{eff}}$ parameter is obtained, consider the case where only pitch damping is taken into account. The case including pitch inertia is merely an extension of the same approach. To keep the example simple, we shall omit consideration of the $C_{m_{(\alpha=0)}}$ and $C_{N_{(\alpha=0)}}$ terms, which would be included in the more general case. These simplified equations are

$$C_m = C_{m_\alpha}\alpha + C_{m_q}(q\bar{c}_w/2V_0) + C_{m_{\delta_e}}\delta_e$$

$$C_L = C_{L_\alpha}\alpha + C_{L_q}(q\bar{c}_w/2V_0) + C_{L_{\delta_e}}\delta_e$$

It was assumed that the normal load factor was developed through a pull-up maneuver. For this situation, the expression relating pitch rate q to normal load factor n is

$$q = (g/V_0)(n-1)$$

The assumption of the approximation $n \approx (S_w q_0/W)C_{L_\alpha}\alpha$ was made. Substituting these expressions in the foregoing equations and taking the partial derivative of each with respect to α produced the following expressions:

$$(\partial C_m/\partial\alpha)_{\text{eff}} = C_{m_\alpha} + C_{m_q}(S_w q_0/mV_0)(\bar{c}_w/2V_0)C_{L_\alpha}$$

$$(\partial C_L/\partial\alpha)_{\text{eff}} = C_{L_\alpha} + C_{L_q}(S_w q_0/mV_0)(\bar{c}_w/2V_0)C_{L_\alpha}$$

From these expressions, the "effective static stability" $(\partial C_m/\partial C_L)_{\text{eff}}$ was formed:

$$\left(\frac{\partial C_m}{\partial C_L}\right)_{\text{eff}} = \frac{C_{m_\alpha} + C_{m_q}C_{L_\alpha}(S_w q_0/mV_0)(\bar{c}_w/2V_0)}{C_{L_\alpha} + C_{L_q}C_{L_\alpha}(S_w q_0/mV_0)(\bar{c}_w/2V_0)}$$

For the configuration studied, $C_{L\alpha}$ proved to be much larger than $C_{L_q}C_{L_\alpha}(S_w q_0/mV_0)(\bar{c}_w/2V_0)$, and so the final form of this last expression could be written as

$$(\partial C_m/\partial C_L)_{\text{eff}} = (\partial C_m/\partial C_L) + C_{m_q}(S_w q_0/mV_0)(\bar{c}_w/2V_0)$$

The pitching moment equation for trim studies could then be written:

$$C_m = (\partial C_m/\partial C_L)_{\text{eff}}C_L + C_{m_{\delta_e}}\delta_e = 0$$

The preceding equation was the basis of the study of the 1.0-g trim and accelerated stability cases. The term involving C_{m_q} was dropped for the 1.0-g trim case (since $q = 0$) but retained for the accelerated stability case.

In order to obtain a relative feel for magnitudes of factors being discussed, the composite curve of Fig. 11 was assembled. The impact of flexibility on the vehicle may be evaluated by comparing the following sets of $(\partial C_m/\partial C_L)_{\text{eff}}$ curves:

1.0-g level flight	flexible no damping to rigid no damping
accelerated stability	flexible with damping to rigid with damping
dynamic stability	flexible with damping and pitch inertia to rigid with damping

Consider first the 1.0-g trim case for the flexible vehicle. Comparing the rigid airplane curve with the flexible airplane curve for "no damping" provides a measure of the effect of the combined flexible aerodynamic loading due to $C_{L\alpha}\alpha$ and translational acceleration inertia loading. These loadings are identified as the biggest flexibility contributors at both weight conditions. Combining these characteristics with the flexible parameters $C_{m_{(\alpha=0)}}$, $C_{L_{(\alpha=0)}}$, C_{L_α}, $C_{m_{\delta_e}}$, and $C_{L_{\delta_e}}$

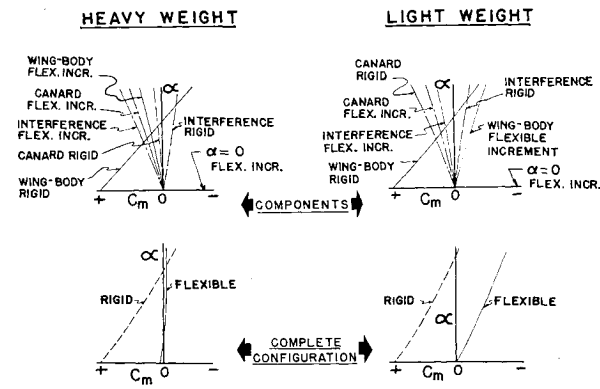

Fig. 10 Pitching moment vs angle-of-attack buildup, flexible and rigid airplane at a high subsonic Mach number; sea-level flight condition.

provides enough information to determine wings level, 1.0-g trim elevator settings, and, consequently, the speed stability for the flexible airplane. The differences noted between the two weight conditions can be attributed to mass distribution loadings differences, as previously discussed.

The curves labeled "with damping" in Fig. 11 are those applicable for determining the accelerated stability characteristics under quasi-steady flight conditions (that is, when pitch acceleration is zero or negligibly small). The largest influence on these flexible vehicle characteristics are those just discussed; however, the flexible vehicle pitch damping components contribute in a significant manner, particularly for the light-weight configuration.

One of the primary reasons for undertaking this phase of the study was to isolate and evaluate the influence of the pitch acceleration inertia loading. Comparing the flexible configuration curves labeled "with damping" with those labeled "with damping and pitch inertia" reveals the magnitude of this factor to be large, more so for the light-weight configuration than for the heavy-weight configuration. These results are of major significance in analyzing the vehicle's dynamic stability and control response characteristics; one of the main characteristics affected is the frequency of the short-period motion.

Although it allowed a closer investigation of these latter short-frequency effects, the direct influence coefficient approach permitted only an approximate check of the magnitude of the factors involved. In short, this is because we have to infer from $(\partial C_m/\partial C_L)_{\text{eff}}$ the character of $(\partial C_m/\partial \alpha)_{\text{eff}}$, which appears directly in the frequency determination. A slight digression into the reasons behind this is in order.

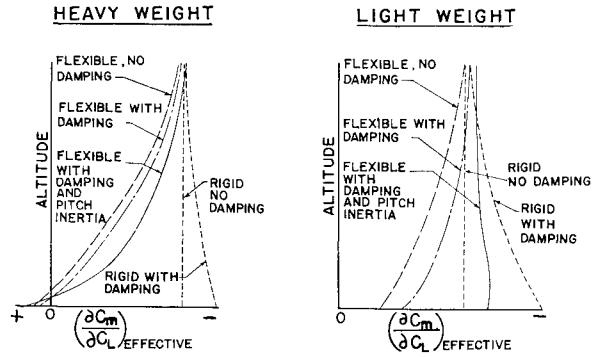

Fig. 11 Effective static stability $(\partial c_m/\partial c_L)_{\text{eff}}$ for complete vehicle, flexible and rigid, illustrating effects of major loads on a canard-delta configuration at a high subsonic Mach number.

The main problem stems from the fact that it is very difficult to obtain readily a transformation relating the angle-of-attack reference used in the influence coefficient problem analyses to the angle-of-attack reference of the dynamic stability problem formulation. In the influence coefficient analyses, the angle-of-attack reference was a line tangent to the wing surface slope at the wing apex. This was a convenient choice, for it permitted the most expedient joining of vehicle component effects to form the whole. In the dynamic stability analyses, the reference line for angle of attack was a body axis related to mass characteristics and rigid vehicle main lifting surface orientation. This axes system was the one for which the equations of motion were written. It is pertinent also to emphasize that this axes system is the same one used for the modal analyses described earlier. For this reason, the difficulty being discussed is avoided in the modal technique and constitutes another advantage in its application in connection with most dynamic aerothermoelastic problems. Although one does know the orientation of the velocity vector (and, consequently, the angle of attack) with respect to the reference system attached at the wing apex, the relationship difficult to define is the angle between the flexible vehicle wing apex axes and the equations of motion axes.

In light of the foregoing reasoning, the most meaningful form of the results of the influence coefficient technique is with respect to a stability axes system expressed in terms of moments and forces. It is for these reasons that, instead of working with C_{m_α}, which is more pertinent to a dynamic stability calculation, $(\partial C_m/\partial C_L)_{\text{eff}}$ is used herein.

To provide a further meaningful relationship between the $(\partial C_m/\partial C_L)_{\text{eff}}$ parameter, including damping and pitch inertia, and the dynamic stability equation formulation, including a pitch inertia loading, let us proceed to a simplified development of the equations of motion. Consider all of the aerodynamic parameters as applicable to the flexible airplane and that the pitch acceleration effect is accounted for separately by additional terms, $C_{N_{\ddot\theta}}$ and $C_{m_{\ddot\theta}}$. The following equations are in a body axes system:

$$(\dot\alpha - \dot\theta)V_0 - g = -(q_0 S_w/m)[C_{N_\alpha}\alpha + C_{N_{\ddot\theta}}\ddot\theta]$$

$$\ddot\theta = (q_0 S_w \bar c_w/I_y)[C_{m_\alpha}\alpha + C_{m_{\dot\theta}}(\dot\theta \bar c_w/2V_0) + C_{m_{\ddot\theta}}\ddot\theta]$$

Based on experience, $C_{N_{\dot\theta}}$ was assumed negligibly small. After taking the Laplace transform of these equations, the characteristic equation may be obtained:

$$S^2 + \frac{\left[\left(\frac{\bar c_w}{2V_0}\right)C_{m_{\dot\theta}} + \left(\frac{q_0 S_w}{mV_0}\right)\left(C_{m_{\ddot\theta}} - \frac{I_y}{q_0 S_w \bar c_w}\right)C_{N_\alpha} + \left(\frac{q_0 S_w}{mV_0}\right)C_{m_\alpha}C_{N_{\ddot\theta}}\right]}{\left(C_{m_{\ddot\theta}} - \frac{I_y}{q_0 S_w \bar c_w}\right)} S + \frac{\left[C_{m_\alpha} + \left(\frac{q_0 S_w}{mV_0}\right)\left(\frac{\bar c_w}{2V_0}\right)C_{N_\alpha}C_{m_{\dot\theta}}\right]}{\left(C_{m_{\ddot\theta}} - \frac{I_y}{q_0 S_w \bar c_w}\right)} = 0$$

This has the form of a typical second-order system:

$$S^2 + 2\zeta\omega_{n_0}S + \omega_{n_0}^2 = 0$$

The principle contributor to the short period frequency $\omega_n = \omega_{n_0}(1-\zeta^2)^{1/2}$ is

$$\omega_{n_0} = \left(\frac{\text{spring constant}}{\text{mass}}\right)^{1/2} = \left(\frac{q_0 S_w \bar c_w (C_{m_\alpha})_{\text{eff}}}{I_y}\right)^{1/2}$$

$$= \left(\frac{q_0 S_w \bar c_w \left\{\dfrac{C_{m_\alpha} + (q_0 S_w/mV_0)(\bar c_w/2V_0)C_{N_\alpha}C_{m_{\dot\theta}}}{[(q_0 S_w \bar c_w/I_y)C_{m_{\ddot\theta}} - 1]}\right\}}{I_y}\right)^{1/2}$$

If it could be assumed that we knew the transform between the equations of motion axes system and the influence coefficient axes system, the foregoing expression for ω_{n_0} can be developed in the latter system under quasi-steady assumptions:

$$C_{m_{\text{total}}} = C_{m_\alpha}\alpha + C_{m_{\dot\theta}}(\dot\theta \bar c_w/2V_0) + C_{m_{\ddot\theta}}\ddot\theta$$

Let

$$\dot\theta = (g/V_0)\Delta n$$

$$\Delta n = (q_0 S_w/W)C_{N_\alpha}\alpha, \ \alpha \text{ measured from 1.0-}g \text{ trim}$$

$$\ddot\theta = (C_{m_{\text{total}}})(q_0 S_w \bar c_w/I_y)$$

Substituting

$$C_{m_{\text{total}}} = C_{m_\alpha}\alpha + (q_0 S_w/mV_0)(\bar c_w/2V_0)\,C_{N_\alpha}C_{m_{\dot\theta}}\alpha + C_{m_{\ddot\theta}}(C_{m_{\text{total}}})(q_0 S_w \bar c_w/I_y)$$

$$C_{m_{\text{total}}} = \frac{C_{m_\alpha}\alpha + (q_0 S_w/mV_0)(\bar c_w/2V_0)C_{N_\alpha}C_{m_{\dot\theta}}\alpha}{-[C_{m_{\ddot\theta}}(q_0 S_w \bar c_w/I_y) - 1]}$$

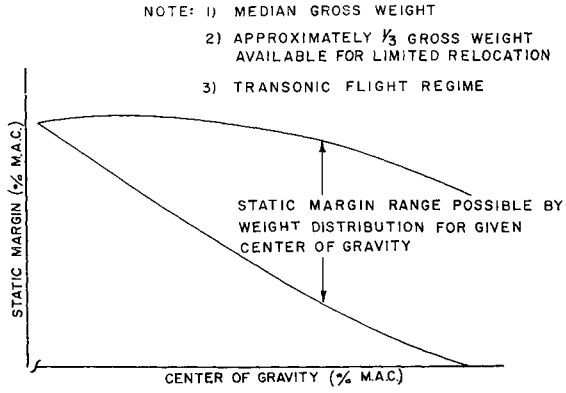

Fig. 12 Static margin available on flexible airplane through realistic mass management.

Taking partial differential with respect to α, one obtains

$$\left(\frac{\partial C_m}{\partial \alpha}\right)_{\text{eff}} = \frac{C_{m_\alpha} + (q_0 S_w/mV_0)(\bar{c}_w/2V_0)C_{N_\alpha}C_{m_{\dot{\theta}}}}{C_{m_{\dot{\theta}}}(q_0 S_w \bar{c}_w/I_y) - 1}$$

This expression is exactly that obtained in the ω_{n_0} for the dynamic problem. (The negative sign disappears in equations of motion formulation.)

The expression for $(\partial C_N/\partial\alpha)_{\text{eff}}$ can be developed in a similar manner neglecting $C_{N_{\dot{\theta}}}$ as small:

$$(\partial C_N/\partial\alpha)_{\text{eff}} = C_{N_\alpha} + C_{N_{\dot{\theta}}}(C_{m_\alpha})_{\text{eff}}(q_0 S_w \bar{c}_w/I_y)$$

From these latter two equations, the parameter plotted in Fig. 11 could be obtained, that is,

$$(\partial C_m/\partial\alpha)_{\text{eff}}/(\partial C_N/\partial\alpha)_{\text{eff}} \approx (\partial C_L/\partial C_m)_{\text{eff with damping and pitch inertia}}$$

With the foregoing as background, it is possible to recognize that $(\partial C_m/\partial C_L)_{\text{eff}}$ is proportional by $(\partial C_L/\partial\alpha)_{\text{eff}}$ to the undamped natural frequency of the short-period motion of the vehicle. Figure 11 reveals that large errors could be made in flexible vehicles' short-period frequency characteristics by neglecting the pitch acceleration inertia loading effects.

A comparison of the "rigid with damping" curve and "flexible with damping and pitch inertia" curve for the light-weight configuration at high altitudes indicates that the flexible vehicle has a shorter period than the rigid vehicle. Prior to obtaining the preceding data, this somewhat unusual situation was observed in calculating the rigid and flexible vehicle short-period frequency using the data obtained from a modal analysis. In fact, this particular analysis obtained the described relationship over a range of altitudes wider than indicated in Fig. 11. This occurred because of the approximate nature (in the context just described) of $(\partial C_m/\partial C_L)_{\text{eff}}$ as an indicator of short-period frequency.

Some Design Implications

Mass Distribution

The foregoing modal flexible-to-rigid-ratio data help to identify design areas where generalizations about mass distribution effects can be made. It does not appear prudent to assume generalizations about the effects of mass distribution on the flexibility contributions to $(C_{N_{(\alpha=0)}})_{\text{wing-body}}$, $(C_{m_{(\alpha=0)}})_{\text{wing-body}}$, $(C_{N_\alpha})_{\text{wing-body}}$, $(C_{m_\alpha})_{\text{wing-body}}$, $C_{NI_{\alpha_c}}$, $C_{mI_{\alpha_c}}$. It does appear possible, however, to say that mass distribution effects are small for flexibility increments associated with rigid forces such as elevon and fore or aft horizontal tail loads that load up the ends of the vehicle. Knowing these facts can save valuable time and effort at the preliminary design level.

The data reflecting the effects of mass distribution on the vehicle's flexible aerodynamic parameters suggested the possibility of mass management to improve these characteristics. As noted, the longitudinal static stability parameter C_{m_α} exhibited the largest impact of mass distribution. This parameter, therefore, became the subject of a mass management study. As discussed in connection with the direct influence coefficient technique, a method was developed which allowed ready buildup of any mass magnitude and/or distribution condition that was within the physical limitations of the vehicle. The degree of variation in stability margin which was attainable through mass management is illustrated as a function of center of gravity for a given gross weight in Fig. 12. Some complication in fuel transfer equipment is implied and must be weighed in design evaluations.

Canard Flexibility

As shown in Fig. 10, the heavy-weight configuration exhibited a neutrally stable pitching moment curve. With the design visibility provided by these data, a means of improving this situation is readily apparent. It is observed that the flexible canard contributes a substantial destabilizing increment. If this could be made to go to zero or contribute a stabilizing increment, a vast improvement in vehicle stability could be realized. This capability is found to exist in the form of the sweep angle of the canard, $\Lambda_{c/4}$. Figure 13 shows the flexible-to-rigid ratio for a lifting surface similar to the canard of Fig. 1 at two different sweep angles; note the greater-than-one flexible-to-rigid ratio for zero sweep and the less-than-one ratio for the swept surface in the transonic region. Considerable design latitude is permitted by these characteristics in attacking the stability problem.

These flexible characteristics of the canard suggest a solution to the elevon reversal problem indicated in Fig. 6. If the characteristics of Fig. 4 could be utilized, a net improvement in maneuver control could be realized. These two characteristics can be brought together through an interconnect of the elevon and canard surface. Figure 14 illustrates the potential improvement possible through this type of arrangement.

Fuselage Divergence and Elevon Reversal

The advent of supersonic and hypersonic vehicles that are many times configured with long slender bodies, often with a canard surface for trim or control, has focused renewed emphasis on the static aeroelastic divergence concept; primary application has been to the fuselage or fuselage-canard combination. Studies of the representative configuration of Fig. 1 have highlighted some of the most interesting characteristics of the behavior and influence of long flexible fuselages.

Classical static aeroelastic divergence considers only structural degrees of freedom, disallowing rigid-body freedom. This restriction generally limits applicability of the concept to component analysis, and in the case of a long

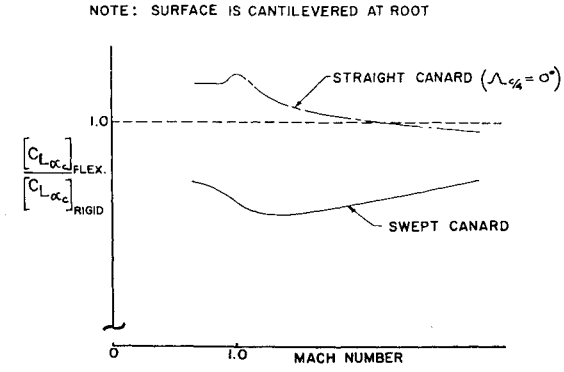

Fig. 13 Effect of sweep angle on canard lift curve slope flexible-to-rigid ratio at sea level.

slender body the restriction is normally satisfied by considering the forebody "built into a brick wall" at some location such as the point of attachment to the wing-afterbody. Although this mathematical model will exhibit divergence, the forces and moments induced by structural deformation will, in the vast majority of cases, be of sufficient magnitude prior to divergence to induce rigid-body motion of the physical system to a degree that negates the artificial "brick wall" boundary conditions. Although some significance is retained for highly localized segments of the structure, it is nevertheless apparent that the forces and moments produced by deformation must be small with respect to the magnitude of forces and moments required to produce motion of the total vehicle in order for classical static aeroelastic divergence to have meaning.

Although this argument generally denies classical static divergence as the direct problem, it should not be construed as an attempt to minimize the importance of aerothermoelasticity to this type of vehicle. Reformulation of the problem with realistic boundary conditions (rigid-body freedom of motion) demonstrates that the same structural flexibility that is fundamental to static divergence reappears as a significant input in other domains, both static and dynamic.

One static problem involving the factors just described is that of steady-state trim control reversal. The direct influence coefficient technique offers a convenient framework for studying this problem. The steady-state longitudinal trim characteristics of a canard configuration with a long flexible fuselage may be represented by the equations shown below:

$$C_{L_{\alpha c}}\alpha_c + C_{L_{\alpha w}}\alpha_w + C_{L_{\delta e}}\delta_e = nW/q_0S_w$$

$$C_{L_{\alpha c}}(l_c/c_w)\alpha_c + C_{L_{\alpha w}}(x_w/\bar{c}_w)\alpha_w + C_{L_{\delta e}}\delta_e(x_e/\bar{c}_w)\delta_e = 0$$

where

$$\alpha_c = \alpha_w + \gamma + \delta_c$$

$$\gamma = (d\gamma/d_{L_c})C_{L_{\alpha c}}(q_0S_w)\alpha_c + (d\gamma/dn)n$$

In order to focus attention on the fuselage influence, the equations have been simplified by omitting unessential aerodynamic loadings and by assuming all components except the fuselage to be rigid.

Solution of these equations for $\delta_{e_{\text{trim}}}$ at 1.0 g, with canard deflection δ_c set to zero, yields

$$\delta_{e_{\text{trim}}} = -\frac{C_{L_{\alpha c}}\frac{l_c}{\bar{c}_w}\left(\frac{W}{q_0S_w} + C_{L_{\alpha w}}\frac{d\gamma}{dn}\right) - C_{L_{\alpha c}}C_{L_{\alpha w}}\frac{x_w}{\bar{c}_w}\frac{d\gamma}{dn} + C_{L_{\alpha w}}\frac{x_w}{\bar{c}_w}\frac{W}{q_0S_w}(1 - \bar{k}_cq_0)}{C_{L_{\alpha c}}C_{L_{\delta e}}\left(\frac{x_e}{\bar{c}_w} - \frac{l_c}{\bar{c}_w}\right) + C_{L_{\alpha w}}C_{L_{\delta e}}\left(\frac{x_e}{\bar{c}_w} - \frac{x_w}{\bar{c}_w}\right)(1 - \bar{k}_cq_0)}$$

where

$$\bar{k}_c = (d\gamma/dL_c)C_{L_{\alpha c}}S_w$$

Similar expressions for α_w and α_c may be derived. The behavior described by these equations for a representative configuration with a long flexible fuselage, triangular wing, and canard with control provided by elevon surfaces on the trailing edge of the wing is illustrated in Fig. 15. The figure illustrates a point of infinite control deflection requirement which is readily identifiable as an elevon reversal, a phenomenon completely analogous to the well-known aileron reversal. This interpretation is justified by the change in direction of the incremental (rigid-to-flexible) deflection above and below the reversal point. The location of the point of control reversal is defined by setting the denominator of the expression for $\delta_{e_{\text{trim}}}$ to zero and solving for q_0, which yields

$$q_{0\text{rev}} = \left(\frac{1}{\bar{k}_c}\right)\frac{(x_e/\bar{c}_w)(C_{L_{\alpha c}} + C_{L_{\alpha w}}) - [C_{L_{\alpha w}}(x_w/\bar{c}_w) + C_{L_{\alpha c}}(l_c/\bar{c}_w)]}{C_{L_\alpha}[(x_e/\bar{c}_w) - ({}_wx/\bar{c}_w)]}$$

The control reversal interpretation may be further verified by noting the disappearance of the singularity when control is provided by a trimmable canard rather than the elevon. Deleting δ_e from the basic equations and solving for $\delta_{c_{\text{trim}}}$ at 1.0 g, we obtain

$$\delta_{c_{\text{trim}}} = \frac{\left(\frac{W}{q_0S_w}\right)\left(\frac{x_w}{\bar{c}_w}\right)(1 - \bar{k}_cq_0) - \left(\frac{d\gamma}{dn}\right)C_{L_{\alpha c}}\left(\frac{x_w}{\bar{c}_w} - \frac{l_c}{\bar{c}_w}\right)}{C_{L_\alpha}\left(\frac{x_w}{\bar{c}_w} - \frac{l_c}{\bar{c}_w}\right)}$$

Isolation of fuselage flexibility as the fundamental mechanism causing this control behavior is readily accomplished by elimination of fuselage flexibility from the formulation of the problem and again noting the disappearance of the singularity.

Figure 15 also indicates the location of the classical aeroelastic divergence speed q_{0D} of the forebody when cantilevered from a position near the apex of the wing. Although some degree of correlation between classical fuselage divergence and elevon reversal is indicated, it is readily demonstrated that the magnitude of q_{0D} varies with the choice of cantilever location, and that q_{0D} is therefore not an adequate criterion

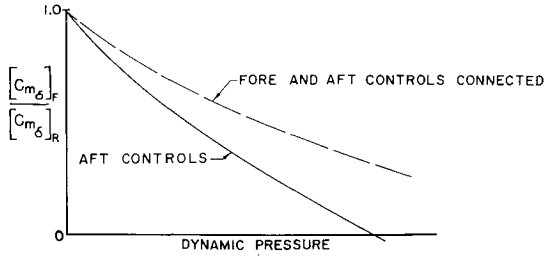

Fig. 14 Improvement in pitch control due to connecting fore and aft control surfaces of a canard-delta airplane at a high subsonic Mach number.

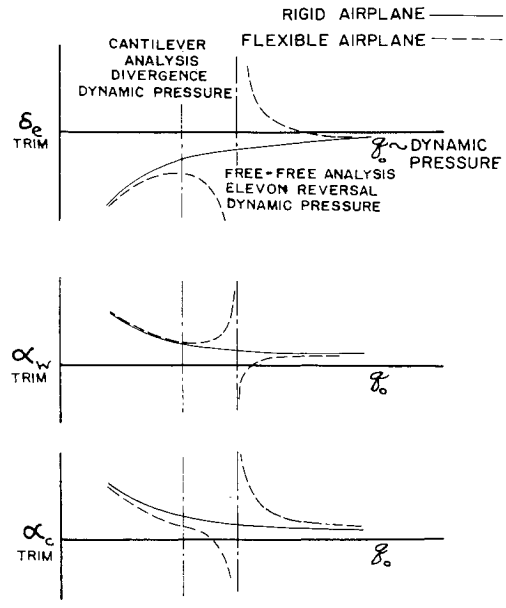

Fig. 15 Effect of flexibility on static longitudinal trim characteristics at a high subsonic Mach number.

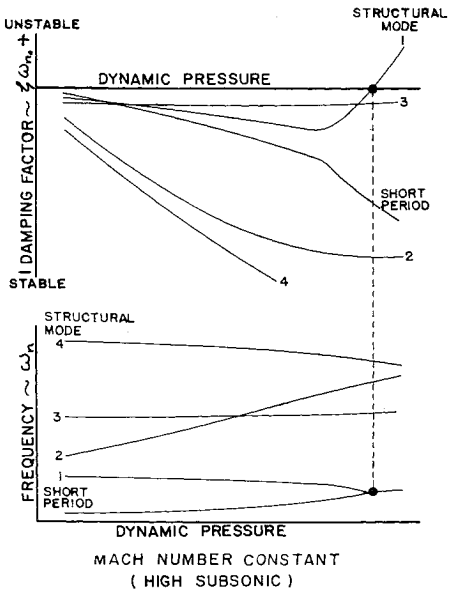

Fig. 16 Structural dynamic instability due to coupling of the longitudinal short period and first symmetric structural mode of a canard-delta airplane.

for the prediction of elevon reversal dynamic pressure. The results obtained by other investigators provide additional verification of this conclusion.[6]

Short Period-Structural Mode Coupling

The forebody flexibility involved in the fuselage divergence-elevon reversal problem was also a factor in producing dynamic coupling between the longitudinal short-period motion and the first structural mode, which was principally fuselage bending. The frequency and damping characteristics of the vehicle response resulting from a modal analysis including pitch and plunge rigid-body modes and four symmetric structural modes are shown in Fig. 16. Selective stiffening of the forebody removed this particular problem.

The foregoing phenomenon is not new; other investigators have discussed various aspects of the problem and attempted to define criteria for preventing this type of dynamic coupling.[7–10] One of the necessary but not sufficient conditions for coupling is the proximity of a structural mode frequency to the short-period mode frequency. With this condition existing, coalescence resulting in an instability is possible.

Control Systems

The modal approach to describing a vehicle's flexible characteristics has much to recommend it for use in studying the vehicle's control system design. As just discussed, vehicles of the type being covered in this paper tend to have structural frequencies close to the short-period rigid-body motion. Since most high-speed air vehicles require a stability augmentation system, a design problem arises from the fact that the required sensing devices measure large structural motion, together with the desired rigid-body motion. In addition, estimates of the rigid-body motion are dependent on accurate aerodynamic data estimates, including proper aerothermoelastic considerations. Another factor pertinent to this discussion is the current tendency toward complexity of control system augmentation system designs, which make it increasingly difficult to come rapidly to grips with potential problem areas. The modal techniques described herein for obtaining flexible-to-rigid ratios that reflect *both inertia and aerodynamic* loadings can be used to describe *concisely* a flexible vehicle's characteristics structurally and aerodynamically to the required degree of accuracy. This may be done by using just enough structural equations (usually one or two) to insure the required accuracy of motion and frequency content and then using flexible-to-rigid aeroelastic corrections to obtain the necessary aerodynamic accuracy, which would ordinarily be missing if only a few structural equations were used. "Residual stiffness" is a term that is often used to describe the stiffness effect over and above that from a small number of modes that would be present in the lower-mode aerodynamic inputs *if* an infinite (or large) number of modes were used (see Refs. 7–9 for a similar approach to residual flexibility.)

Conclusions

The results of this study have shown the potentially extensive impact of aerothermoelastic factors on the stability and control characteristics of a typical low load factor-low mass fraction aerospace vehicle. The impact of aerothermoelasticity on the flutter characteristics of such a vehicle are known to be equally extensive. A major controlling design parameter in both problem areas is vehicle stiffness. Since a strong connection exists between stiffness and weight, it is apparent that the most efficient use of weight in a vehicle's design will only come about through more coordinated and more detailed analyses in these two design areas. Much about the nature of each exists to encourage this: structural influence coefficients used in one can be used in the other; mass distribution definitions for one can be used in the other; mode shapes used for one can be used in the other; and aerodynamic data for one, in many instances, can be used in the other. Although it is currently possible to obtain structural influence coefficients at the preliminary design level, recent direct analog computer developments and companion digital program developments offer encouragement that more detailed and accurate data can be obtained in an even more compressed time period. Research and development effort augmenting this work would be well spent.

References

[1] Wykes, J. H., Sweet, H. R., Joseph, J. A., and Hodson, C. H., "Commercial supersonic transport flutter studies," Aeronautical Systems Div. TDR-63-818 (May 1964).

[2] Bisplinghoff, R. L., Ashley, H., and Halfman, R. L., *Aeroelasticity* (Addison-Wesley Publishing Co., Inc., Cambridge, Mass., 1955).

[3] Fung, Y. C., *An Introduction to the Theory of Aeroelasticity* (John Wiley and Sons, Inc., New York, 1955).

[4] Skoog, R. B. and Brown, H. H., "A method for the determination of the spanwise load distribution of a flexible swept wing at subsonic speeds," NACA TN 2222 (March 1951).

[5] Falkner, V. M., "The calculation of aerodynamic loading on surfaces of any shape," British Repts. and Memo. 1910 (August 26, 1943).

[6] Etkin, B., "Lift distribution on supersonic wings with subsonic leading edges and arbitrary angle of attack distribution," J. Aeronaut. Sci. 21, 783–785 (1954); also "Lift distributions on warped wings," Can. Aeronaut. J., 16–20 (April 1955).

[7] Schwendler, R. G. and MacNeal, R. H., "Optimum structural representation in aeroelastic analyses," Aeronautical Systems Div. TR-61-680 (March 1962).

[8] Schwendler, R. G. and Hill, J. H., "Low frequency instabilities of free systems," Aeronautical Systems Div. TR-63-655 (November 1963).

[9] Pearce, B. F., Siskind, R. K., Pass, H. P., and Wolkovitch, J., "Topics on flexible airplane dynamics," Aeronautical Systems Div. TDR-63-334, Vol. I, *Residual Stiffness Effects in Truncated Modal Analysis*; Vol. II, *The Application of Flexible Transfer Approximations and Sensitivity of Airframe*; Vol. III, *Coupling of the Rigid and Elastic Degrees of Freedom of an Airframe*; Vol. IV, *Coupling of the Rigid and Elastic Degrees of Freedom of an Airframe-Autopilot System* (July 1963).

[10] Frueh, F. J. and Zisfeim, M. B., "Numerical approximation method for flexible vehicle transfer function factors," Aeronautical Systems Div. TR-62-1063 (March 1963).